J. Electrochem. Sci. Eng. **13(3)** (2023) 521-536; http://dx.doi.org/10.5599/jese.1657

Open Access : : ISSN 1847-9286
https://pub.iapchem.org/ojs/index.php/JESE

Original scientific paper

γ-Fe_2O_3 silica-coated 2-(2-benzothiazolyl azo)-4-methoxyaniline for supercapacitive performance

Jinan Mohammed Mahmood[1], Zaid H. Mahmoud[1,✉], Noor Sabah Al-Obaidi [1] and Ahmed M. Rahima[2]

[1]*Chemistry Department, College of Science, Diyala University, Iraq*
[2]*Chemistry Department, College of Science, Mustansiriyah University, Iraq*

Corresponding author: ✉zaidhameed_91@yahoo.com

Received: December 30, 2022; Accepted: January 30, 2023; Published: February 6, 2023

Abstract

Magnetic γ-Fe_2O_3@SiO_2 core-shell nanocomposite was prepared using Stöber method and functionalized firstly by isopropenyloxytrimethylsilane as a coupling agent to enter active acetylacetone on the surface of nanoparticles, and after that by the synthesized azo dye ligand, 2-(2-benzothiazolyl azo)-4-methoxyaniline. In such a way, γ-Fe_2O_3@SiO_2-azo dye hybrid nanocomposite was formed. The structure of the synthesized azo dye was evidenced by physical and chemical analysis using melting point, Fourier-transform infrared spectroscopy (FT-IR), CHNS elemental analysis, proton nuclear magnetic resonance (HNMR) and gas chromatography mass spectrometry (GC-MS). The magnetic properties, structure, element composition and morphology characterization of prepared materials (γ-Fe_2O_3, γ-Fe_2O_3@SiO_2, and γ-Fe_2O_3@SiO_2-azo dye) were investigated by vibrating sample magnetometer (VSM), X-ray diffraction (XRD), X-ray photoelectron spectroscopy (XPS), transmission electron spectroscopy (TEM) and field electron scanning electron microscopy-energy dispersive X-ray-mapping techniques. The electrochemical performance of synthesized γ-Fe_2O_3, γ-Fe_2O_3@SiO_2, and γ-Fe_2O_3@SiO_2-2-(2-benzothiazolyl azo)-4-methoxyaniline) electrodes were carried out using cyclic voltammetry (CV), galvanostatic charge-discharge (GCD) and electrochemical impedance spectroscopy (EIS). It was shown that the finally prepared γ-Fe_2O_3@SiO_2-2-(2-benzothiazolyl azo)-4-methoxyaniline) hybrid nanocomposite electrode possesses good storage charge capability of 580 F g^{-1} at 1 A g^{-1}.

Keywords

Hybrid nanocomposite; maghemite nanoparticles; azo dye ligand; supercapacitor electrode; coatings

Introduction

Supercapacitor (SC) is a storage energy device with long cycle life, high power density and fast recharge capability, but in spite of many advantages, SCs still suffer from the low density of energy

before they could have authentic electric applications [1,2]. SC is composed of two electrodes (anode and cathode), membrane and electrolyte solution. Different metal oxides, sulfides [3], hydroxides [4], and metal complexes [5] have already been studied as electrode materials to improve the capacitance of SC. In order to attain high efficiency, two electrodes should store the energy or charges equally, which means that if one electrode stores charge more than the other, it will cause a difference in the charge balance of the electrodes of SC [6].

Maghemite phase (γ-Fe_2O_3) is a one of the auspicious electrode materials because of its natural abundance and large specific capacitance [7,8]. The electrochemical behavior of iron oxide [9] and iron oxide coated by SiO_2 have already been examined, but without reporting their supercapacitance or electrochemical performance [10-12]. However, their chemical stability, good theoretical capacitance and low cost have resulted in protracted studies targeted to improve the electrochemical properties of iron oxides. The studies reported that as high as 207 F g^{-1} specific capacitance for iron oxide prepared from ultrasonic method [13]. We believe that incorporating of γ-Fe_2O_3 with ligand compounds nanocomposite may be an effective method to enhance electrochemical properties and performance [14,15]. So, the maghemite/ligand hybrid nanocomposite will be more committing electrode for supercapacitor than pure maghemite. In this paper, we report the synthesis of azo dye on the surface of silica-coated magnetic maghemite nanoparticles incorporated with 2-(2-benzothiazolyl azo)-4-methoxyaniline ligand as new nanomagnetic electrodes for supercapacitor applications.

Experimental

Materials

In this work, the reagents and solvent were purchased from Fisher Scientific and Sigma-Aldrich with 98 % purity, while other chemical materials were supplied from Fluka. All chemicals were used without purification.

Preparation of azo dye ligand

A mixture (10 ml ethanol, 2 ml conc. HCl) has been used to melt of (0.335 g, 1 mM) of 2-aminobenzothiazole, and diazotized with 10 % solution of $NaNO_2$ at 5 °C. The mixture was added gradually with stirring to cool ethanolic solution (0.307 g, 1 mM) of 4-methoxyaniline. After that, 25 ml of 1 M NaOH solution was added to the colored mix and azo ligand was precipitated, filtrated and washed various times with (1:1) C_2H_5OH: H_2O, and left to dry. The reaction is shown in Scheme 1. Some other physical characteristics of the synthesized azo-dye are summarized as follows.

Color: deep brown. M.P. = 300 °C >. ^{1}H NMR (400 MHz, DMSO-d6): δ = 7.00-7.857 (m, 6H), 7.908 (s, 2H) (NH_2), 3.426 (s, 3H) (OCH_3). IR (cm^{-1}): ν (N-H) = 3387-3441, ν (C=N) = 1604, ν (C=C) = 1504, ν (N=N) = 1535 and 1568, $\delta_{as,s}$ CH_3 = 1404 and 1387, 1309. λ_{max} = 240, 354 and 412 nm. Elemental analysis calculated: C 58.92 %, H 3.92 %, N 18.98 %, O 4.98 %, S 10.92 %.

Preparation of magnetic γ-Fe_2O_3 nanoparticles

Potassium ferric oxalate $K_3[Fe(C_2O_4)_3]\cdot 3H_2O$ was used as a source for synthesis of γ-Fe_2O_3 nanoparticles by photolysis method [16-18]. In a 125 W irradiation system, 1 g of ferric complex solution was irradiated for 30 min until a yellow precipitate of ferrous oxalate was formed. The precipitate was decanted, washed with distilled water and dried at 80 °C for 4 h. The dried precipitate was burned at 400 °C for 2 h.

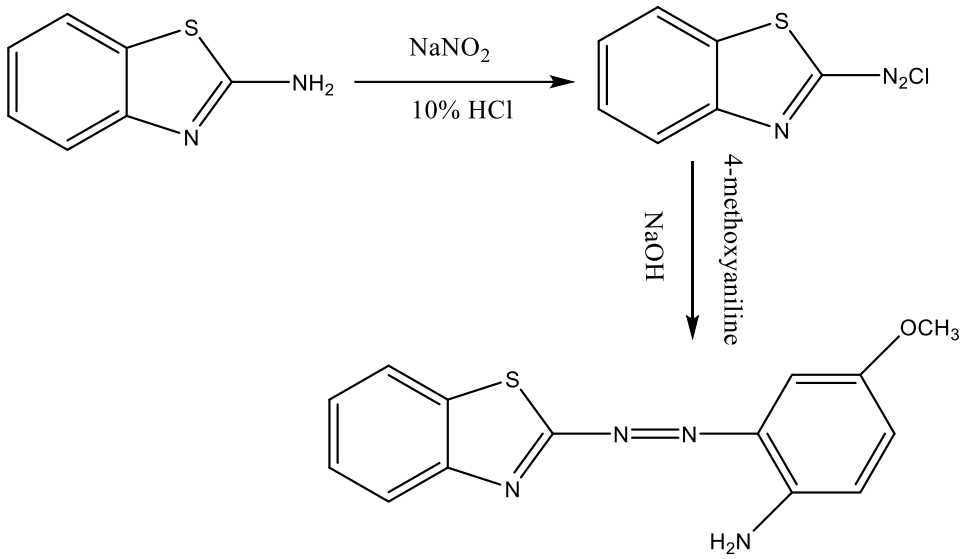

Scheme 1. *Preparation of azo ligand*

Preparation of γ-Fe_2O_3@SiO_2@IPTMS

The preparation of γ-Fe_2O_3@SiO_2@ consists of two steps:

The first step consists of dispersing 0.5 g of the brown magnetic precipitate of γ-Fe_2O_3 in the mixture of water and 2-propanol with a ratio of 1:10 with stirring for 2 h at 22 °C. The mixture of oleic acid (10 ml), ammonium solution (28 %, 5 ml), distilled water (10 ml) and 5 ml of tetraethyl orthosilicate (TEOS) was added to the dispersing mixture under continuous stirring. The product was magnetically isolated and dried at 80 °C for 2 h, and used in the next step. The second step was carried out by dispersing 1 g of γ-Fe_2O_3@SiO_2 in 50 ml of 70 % ethanol solution by sonication process for 1 h. Then 2 ml of (3-iodopropyl)trimethoxysilane (IPTMS) was added to the mixture under a continuous stirrer. Finally, the product was magnetically isolated and dried at 80 °C for 2 h.

Preparation of γ-Fe_2O_3@SiO_2-2-(2-benzothiazolyl azo)-4-methoxyaniline

Firstly, (0.1 g) γ-Fe_2O_3@SiO_2@acetylacetone (synthesized from refluxed γ-Fe_2O_3@SiO_2@IPTMS with pentane-2,4-dione in the presence of sodium hydride) was dispersed in 10 ml mixture of water and ethanol with ratio (1:1) for 30 min. Then, 0.2 g of 2-(2-benzothiazolyl azo)-4-methoxyaniline was added to the dispersion mixture and refluxed for 10 h. After that, the functionalized magnetic nano-composite was separated by pieces of magnetic bar. Finally, it was washed several times with acetone and distilled water and dried at 80 °C for 3 h. All processes and prepared compounds are summarized in Scheme 2.

Electrochemical measurements

The electrochemical cell contained three electrodes, *i.e.,* 1×1 cm pieces of prepared samples as working electrodes, Ag/AgCl (saturated KCl) as the reference electrode and Pt foil as the counter electrode. 1 M Na_2SO_4 was utilized as the electrolyte solution. The active material(s) (85 %), carbon black (10 %) and polyvinyl fluoride (5 %) were mixed by using a few drops of N-methyl-2-pyrrolidione solvent to obtain mixtures that were coated on the foil of graphite substrate (1 cm^2) and dried in an oven for 10 h at 70 °C. The mass of active materials (γ-Fe_2O_3, γ-Fe_2O_3@SiO_2, and γ-Fe_2O_3@SiO_2- azo dye) on each of thus formed working electrodes was approximately 0.5 g. The three electrodes were utilized to examine the pesudocapacitive performance of prepared samples in terms of cyclic voltammetry (CV), galvanostatic charge-discharge (GCD) and electrochemical impedance spectroscopy

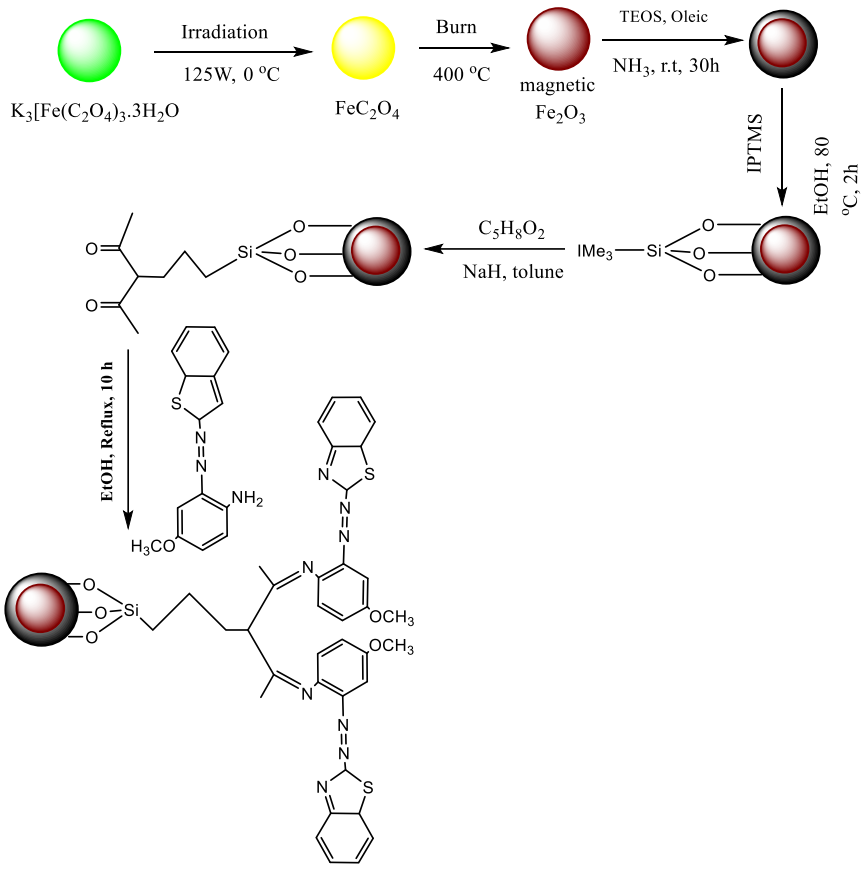

Scheme 2. *Steps during preparation of γ-Fe_2O_3@SiO_2-2-(2-benzothiazolyl azo)-4-methoxyaniline*

Results and discussion

Azo ligand characterization

The 2-(2-benzothiazolyl azo)-4-methoxyaniline azo ligand was characterized using fragmentation electron effect. The results of hit mass spectroscopy (Figure 1) illustrated that the molecular weight of the $C_{14}H_{12}N_4OS$ ligand is 284 g mol^{-1}. Peak at *m/z* = 284 is assigned to [M]+ and correlated with the prepared azo ligand. Set of peaks located at 210, 134, 77.2 and 35 are related to other fragmentation. The main fraction supported with cracking product is shown in Scheme 3.

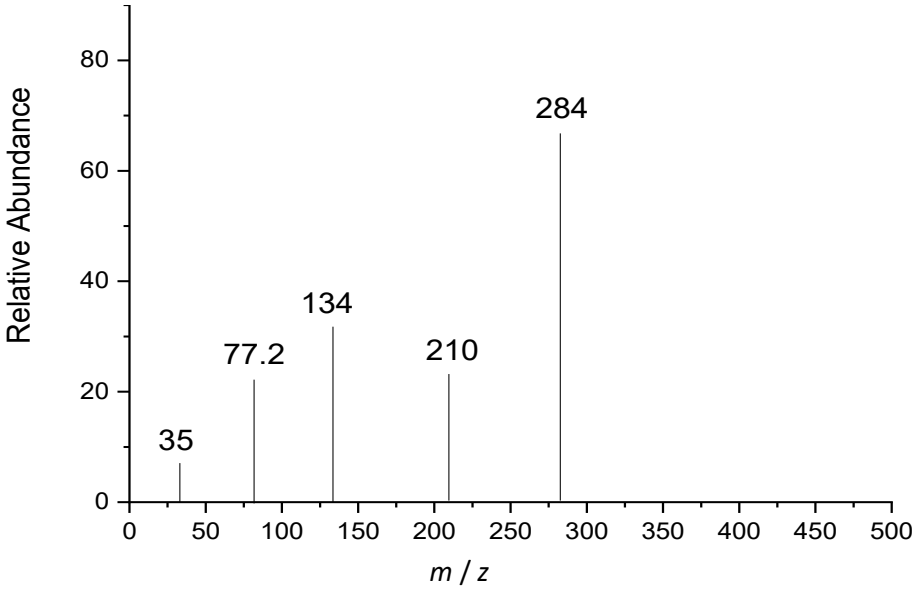

Figure 1. *Mass spectrum of azo ligand*

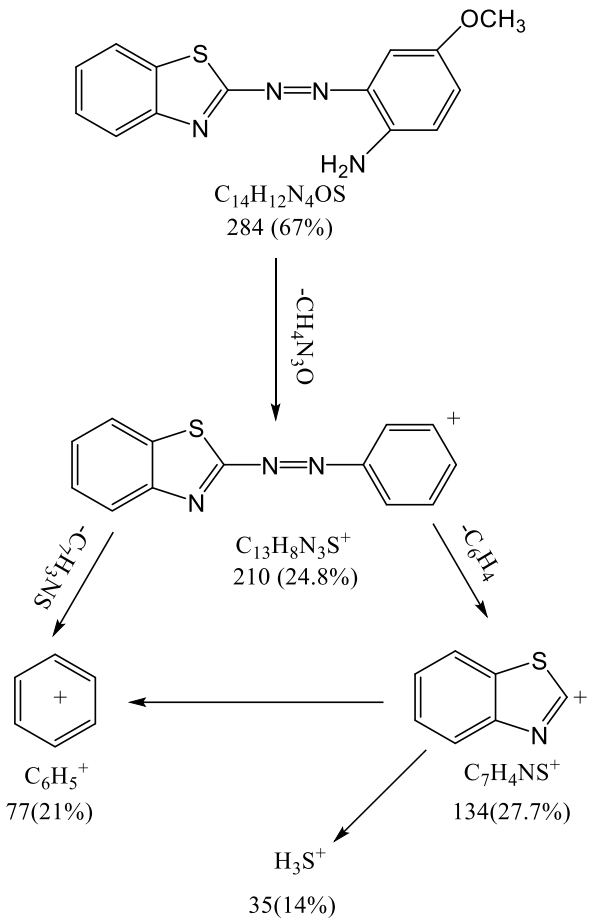

Scheme 3. *Fragmentation pattern of azo ligand*

Magnetic properties

The magnetic properties of prepared materials were investigated by vibrating sample magnetometry (VSM). The magnetization plots of γ-Fe_2O_3, γ-Fe_2O_3@SiO_2 and γ-Fe_2O_3@SiO_2-2-(2-benzothiazolyl azo)-4-methoxyaniline are shown in Figure 2. The results show that the saturation magnetization is equal to 25-40 emu g^{-1} without any hysteresis loop. In addition, the results show quick ascension in magnetization curves without any coercivity and the samples show supermagnetic behavior at room temperature. These magnetic properties of prepared nanoparticles are pivotal in their applications since they prevent aggregation of particles and enable their re-dispersion in the reaction medium in the absence of a magnetic field [19].

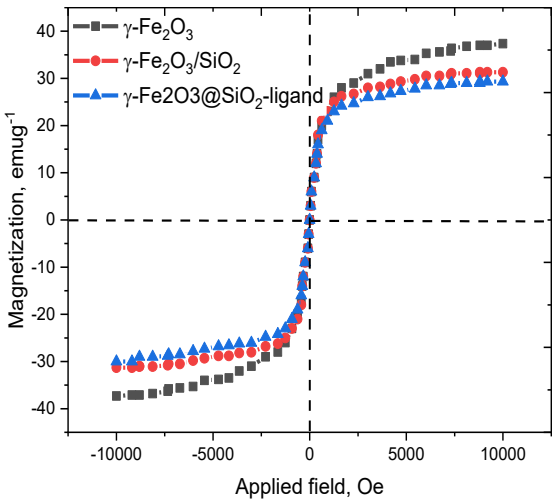

Figure 2*. VSM of prepared electrode materials*

Structure characterization

The structure properties of γ-Fe_2O_3, γ-Fe_2O_3@SiO_2 and γ-Fe_2O_3@SiO_2-2-(2-benzothiazolyl azo)-4-methoxyaniline were evaluated by XRD and XPS. The XRD of γ-Fe_2O_3, γ-Fe_2O_3@SiO_2, azo ligand 2-(2-benzothiazolyl azo)-4-methoxyaniline, and γ-Fe_2O_3@SiO_2-2-(2-benzothiazolyl azo)-4-methoxyaniline are presented in Figure 3A-D, respectively. The results in Figure 3A show diffraction peaks located at 30.1, 35.6, 43.2, 53.4, 57.1 and 62.5°, which correspond to face-centered cubic (220), (311), (400), (422), (511) and (440) crystalline planes, in agreement with (JCPDS-39-1340). On the other side, the results (Figure 3B) show a new diffraction peak centered at 22.8°, which corresponds to (110) plane of amorphous SiO_2. By comparing diffraction peaks of γ-Fe_2O_3 and γ-Fe_2O_3@SiO_2, it was found that the coated SiO_2 doesn't change the structure of γ-Fe_2O_3. As can be seen (Figure 3D), the presence of sharp peaks confirms that the structure of γ-Fe_2O_3@SiO_2 remains crystalline after being coated with a layer of azo ligand [20,21].

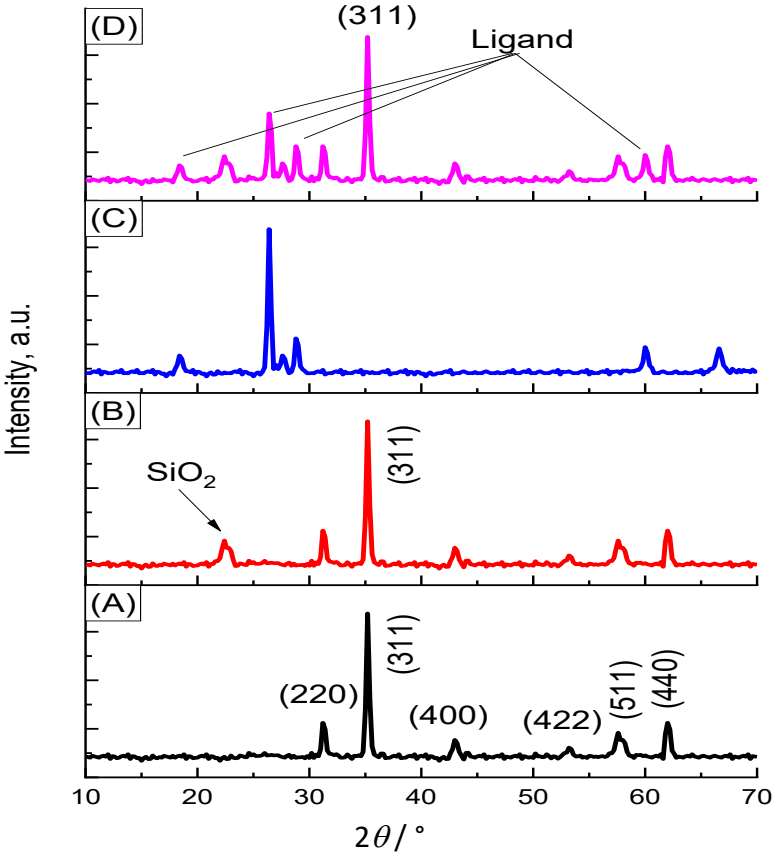

Figure 3. *XRD patterns of: (A) γ-Fe_2O_3, (B) γ-Fe_2O_3@SiO_2, (C) azo ligand, and (D) γ-Fe_2O_3@SiO_2-azo ligand*

The chemical composition of γ-Fe_2O_3, γ-Fe_2O_3@SiO_2 and γ-Fe_2O_3@SiO_2-2-(2-benzothiazolyl azo)--4-methoxyaniline was characterized using XPS. The XPS of prepared compounds corresponding to C, N, O, Si, S and Fe energy levels are presented in Figures 4A to 4F. The energy level of C (Figure 4A) shows three peaks located at 283.5, 286.2 and 289.1 eV corresponding to C-C, C=N and C=C bonds, respectively, which confirm bonding C of acetylacetone and N of 2-(2-benzothiazolyl azo)-4-methoxyaniline ligand [22,23]. The spectrum energy level of N 1s is illustrated at Figure 4B. The spectrum can be deconvoluted to 398.4, 399.5 and 401.2 eV, corresponding to [-C=N-], [-N=N-] and [-NH-], respectively [24]. At 531.8 eV, the energy level spectrum is shown (Figure 4C), which is related to O 1s, confirming the presence of O^{2-} in the composite [25]. As shown in Figure 4D, the characteristic peak of Si 2p is clearly formed at 103.2 eV, which indicates the successful coating of SiO_2 around γ-Fe_2O_3.

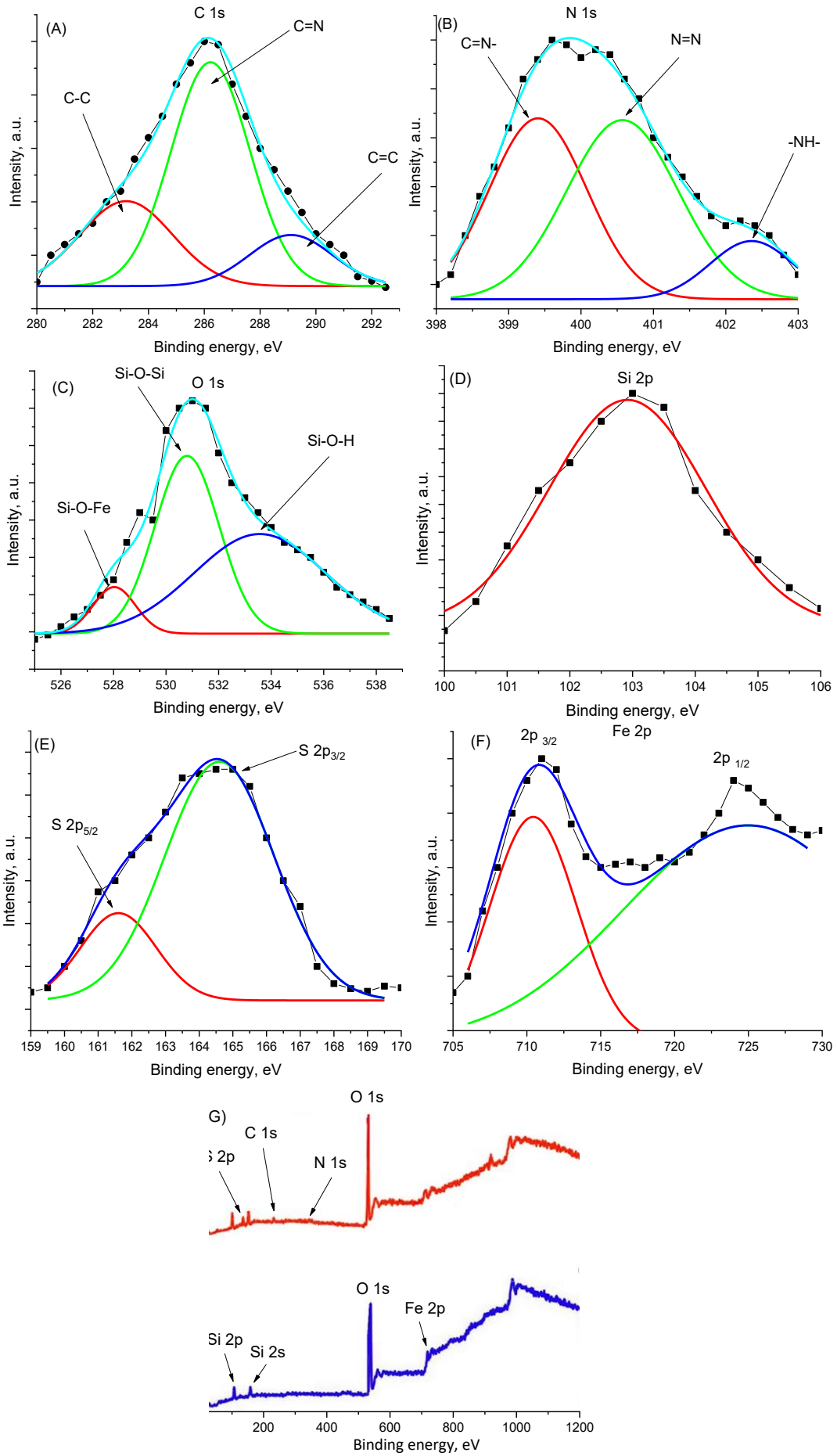

Figure 4. *XPS of: (A) C 1s, (B) N 1s, (C) O 1s, (D) Si 2p, (E) S 2p, (F) Fe 2p, γ-Fe_2O_3@SiO_2-azo dye and (G) survey spectra of γ-Fe_2O_3@SiO_2 and γ-Fe_2O_3@SiO_2-2-(2-benzothiazolyl azo)-4-methoxyaniline*

When comparing the survey spectrum of γ-Fe_2O_3@SiO_2 and γ-Fe_2O_3@SiO_2-2-(2-benzothiazolyl azo)-4-methoxyaniline (Figure 4e), a new peak centered at 145.67 eV is found, corresponding to level energy spectrum of S 2p. This indicates the successfully incorporated ligand with γ-Fe_2O_3@SiO_2. On the other side, the survey spectrum of prepared compounds shows a small peak of Fe, which approves the coating of Fe_3O_4 by SiO_2.

Morphology characterization

The morphology of γ-Fe_2O_3, γ-Fe_2O_3@SiO_2 and γ-Fe_2O_3@SiO_2-2-(2-benzothiazolyl azo)-4-methoxyaniline were performed utilizing TEM, FESEM and EDX-mapping. TEM images of prepared compounds are shown in Figures 5A to 5C.

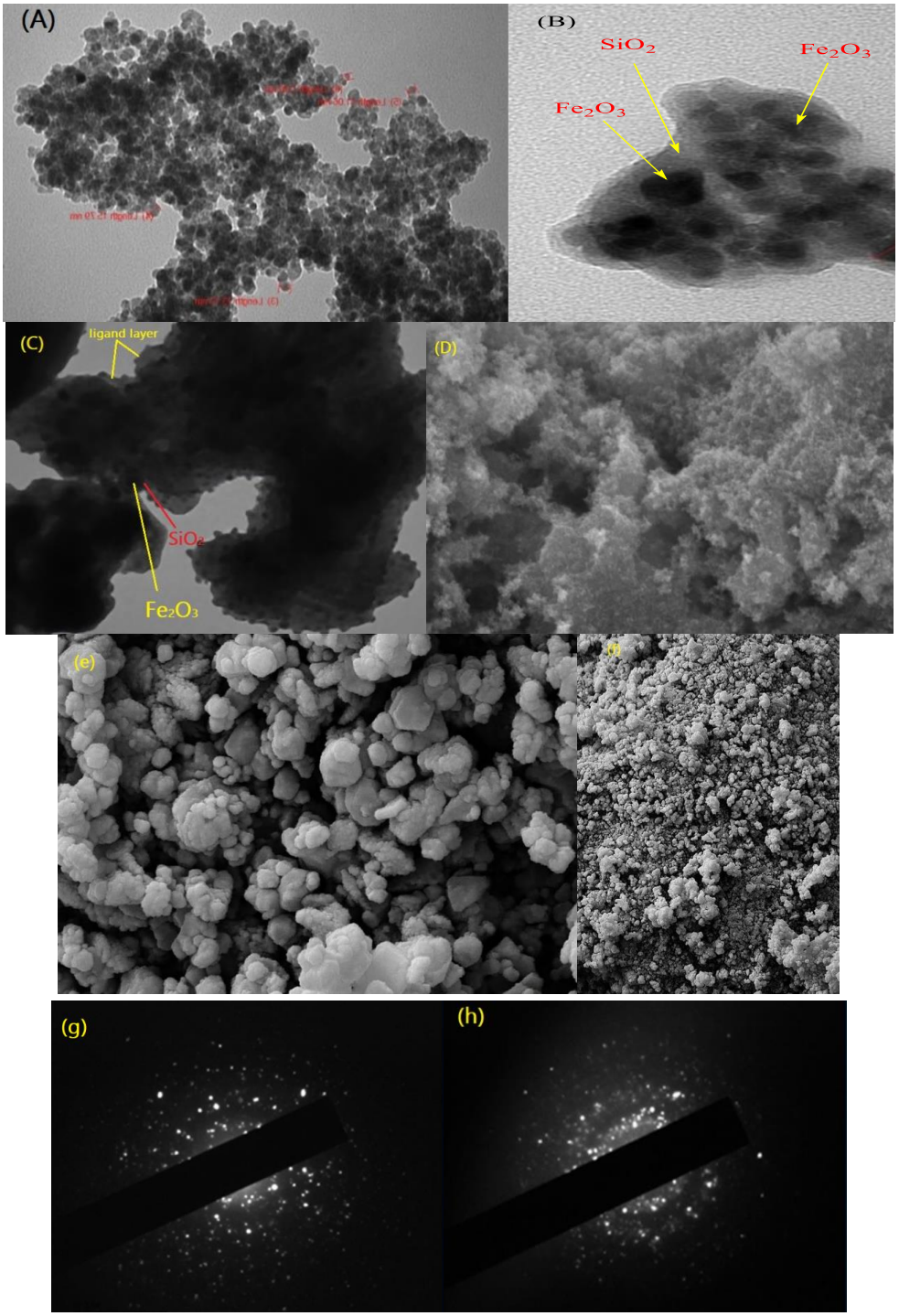

Figure 5. *TEM images of (A) γ-Fe_2O_3, (B) γ-Fe_2O_3@SiO_2, (C)γ-Fe_2O_3@SiO_2-azo ligand; FESEM images of (D)γ-Fe_2O_3, (e) γ-Fe_2O_3@SiO_2, (f)γ-Fe_2O_3@SiO_2-azo ligand, and SAED images of: (g) γ-Fe_2O_3, (h)γ-Fe_2O_3@SiO_2-azo ligand*

The results (Figure 5A) clearly display agglomerates of spherical γ-Fe_2O_3 nanoparticles with 11 nm grain size. TEM images illustrate the core-shell system structure of γ-Fe_2O_3@SiO_2 and confirm the perfect coating of γ-Fe_2O_3 nanoparticles by SiO_2, as shown in Figure 5B. On the other side, the results (Figure 5C) illustrate the complete surrounding of 2-(2-benzothiazolyl azo)-4-methoxyaniline layer around γ-Fe_2O_3@SiO_2, which indicates success in the preparation of the final compound. The microscope evaluation of γ-Fe_2O_3, γ-Fe_2O_3@SiO_2 and γ-Fe_2O_3@SiO_2-2-(2-benzothiazolyl azo)-4-methoxyaniline were investigated using FESEM. The FESEM images of prepared compounds are shown in Figure 5d-f. The results (Figure 5D) show that the magnetic γ-Fe_2O_3 particles were formed in uniform shapes with apparent agglomeration due to their magnetic properties. Added SiO_2 to magnetic γ-Fe_2O_3 makes the shapes of catalyst nanoparticles spherical (Figure 5e). The FESEM images of γ-Fe_2O_3@SiO_2-2-(2-benzothiazolyl azo)-4-methoxyaniline show nanocomposite with a small agglomeration of particles, which may be back to fictionalized of γ-Fe_2O_3 by 2-(2-benzothiazolyl azo)-4-methoxyaniline layer. The results of FESEM are in agreement with XRD and TEM results. The lattice fingers of γ-Fe_2O_3 and γ-Fe_2O_3@SiO_2-2-(2-benzothiazolyl azo)-4-methoxyaniline are shown in Figure 5g-h. The results show the highly crystalline nature of γ-Fe_2O_3@SiO_2-azo, as well as the well-organized dots and ring (Figure 5h), prove the crystalline nature of synthesized material that could be beneficial in structure retention for long-term stability. On the other side, a large number of gleam spots (Figure 5h) compared with pure γ-Fe_2O_3 (Figure 6g) elucidates the coating of γ-Fe_2O_3 by SiO_2 [27,28].

The chemical composition of γ-Fe_2O_3@SiO_2-2-(2-benzothiazolyl azo)-4-methoxyaniline was investigated by element mapping patterns, while compositions of γ-Fe_2O_3 and γ-Fe_2O_3@SiO_2 were carried out by EDX analysis. The EDS spectrum result (Figure 6) of γ-Fe_2O_3@SiO_2-2-(2-benzothiazolyl azo)-4-methoxyaniline shows detectable singles back to Fe, O, Si, S, N and S, as well as the weight percentage of detecting elements, suggesting that the nanocomposite was successfully prepared

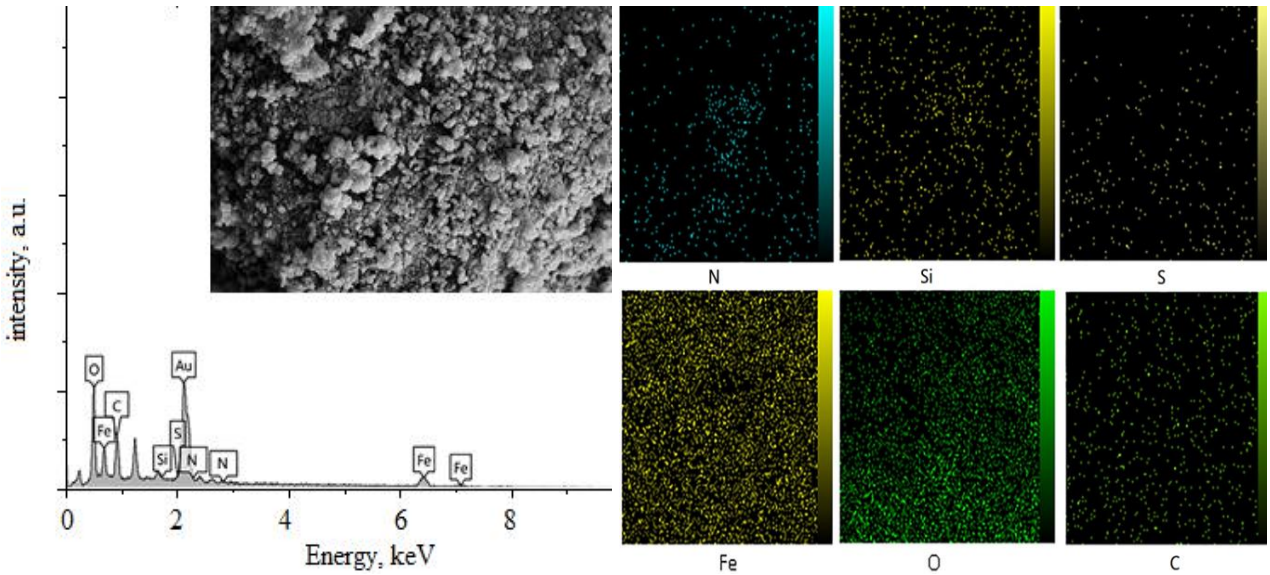

Figure 6. *EDS spectrum of γ-Fe_2O_3@SiO_2-2-(2-benzothiazolyl azo)-4-methoxyaniline and mapping of Fe, Si, S, N, O, C*

The EDX spectra of γ-Fe_2O_3 and γ-Fe_2O_3@SiO_2 are shown in Figure 7. Clear peaks related to Fe and O without other peaks are evident in Figure 7A, which indicates the successful preparation of pure ferric oxide. A new peak related to Si can be detected from EDS analysis after the coating of Fe_2O_3 by SiO_2 (Figure 7B).

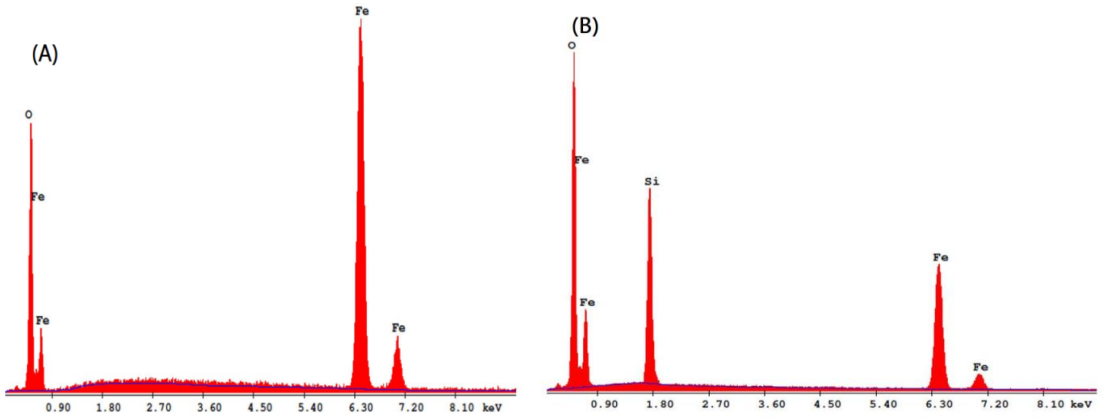

Figure 7. *EDX spectra of: (A) γ-Fe_2O_3 and (B) γ-Fe_2O_3@SiO_2*

BET analysis

The specific area, mean size of particles and the volume of pores for γ-Fe_2O_3 and γ-Fe_2O_3@SiO_2-2--(2-benzothiazolyl azo)-4-methoxyaniline were investigated using BET analysis, and the results are summarized in Table 1. The results show that the surface area of γ-Fe_2O_3 and γ-Fe_2O_3 functionalized by SiO_2 and azo compound was 99.3 and 275.5 m^2/g, respectively, meaning that the functionalized compound has higher surface area due to the presence of silica and azo dye and so, higher capacity for adsorption of species on the electrode surface. In addition, the results demonstrated that the mean pore size of γ-Fe_2O_3 and γ-Fe_2O_3@SiO_2-2-(2-benzothiazolyl azo)-4-methoxyaniline are 3.9 and 4.3 nm, respectively. According to the IUPAC categories, both prepared electrode materials can be classified into mesopores group [29,30].

Table 1. *Nitrogen sorption characteristics of prepared electrode materials*

Electrode material	S_{BET} / $m^2 g^{-1}$	Pore volume, cm^3/g	Average pore diameter, nm
γ-Fe_2O_3	99.3	2.66	3.9
γ-Fe_2O_3@SiO_2-2-(2-benzothiazolyl azo)-4-methoxyaniline	275.5	4.9	4.3

Electrochemical performance

The electrochemical properties of γ-Fe_2O_3, γ-Fe_2O_3@SiO_2 and γ-Fe_2O_3@SiO_2-2-(2-benzo thiazolyl azo)-4-methoxyaniline electrodes were investigated using CV, GCD and EIS techniques. The specific capacitances of three electrodes in the presence 1 M Na_2SO_4 as electrolyte solution were calculated using cyclic voltammetry data. The CVs of prepared compounds were recorded at different scan rates and within 0-1.2 V potential window, as presented in Figure 8. The CVs of γ-Fe_2O_3, γ-Fe_2O_3@SiO_2 and γ-Fe_2O_3@SiO_2-2-(2-benzothiazolyl azo)-4-methoxyaniline examined at 10 mV s^{-1} are shown in Figure 8A. The results demonstrate redox peaks for γ-Fe_2O_3@SiO_2-2-(2-benzothiazolyl azo)-4--methoxyaniline electrode. In addition, the CV result of γ-Fe_2O_3@SiO_2 showed significant improvement when its surface was modified with 2-(2-benzothiazolyl azo)-4-methoxyaniline, and higher specific capacitance was observed. The CVs of γ-Fe_2O_3@SiO_2- 2-(2-benzothiazolyl azo)-4-methoxyaniline at different scan rates are presented in Figure 8B. The results show redox peaks until the highest scan rates with slight shifting, which indicates good electrode capability. On the other hand, the separation of current peaks raised with the rising scan rate because the redox peaks change with reversible reactions between the electrode and electrolyte solution [31]. The specific capacitance (C_{sp}) of prepared electrodes was evaluated by using equation)1) [32]:

$$C_{sp} = \frac{A}{2\nu m \Delta V} \quad (1)$$

where A is the area under plot, ν / V s^{-1} scan rate, m / g is the active mass of the electrode, and ΔV is a potential window. The results are shown in Figure 8C. The results exhibit that the modified γ-Fe_2O_3@SiO_2 by azo ligand (2-(2-benzothiazolyl azo)-4-methoxyaniline) has higher specific capacitance than γ-Fe_2O_3@SiO_2 and γ-Fe_2O_3, because of the interaction between the ferric oxide and azo ligand, which makes the structure of electrode superior and easy for Na_2SO_4 electrolyte solution accessibility. The specific capacitance of prepared electrodes was also examined at different scan rates 10-100 mV s^{-1} and the results are also presented in Figure 8C. The results show a reduction in specific capacitance values with increasing scan rate because of difficult redox transition at high scan rate value [33,34].

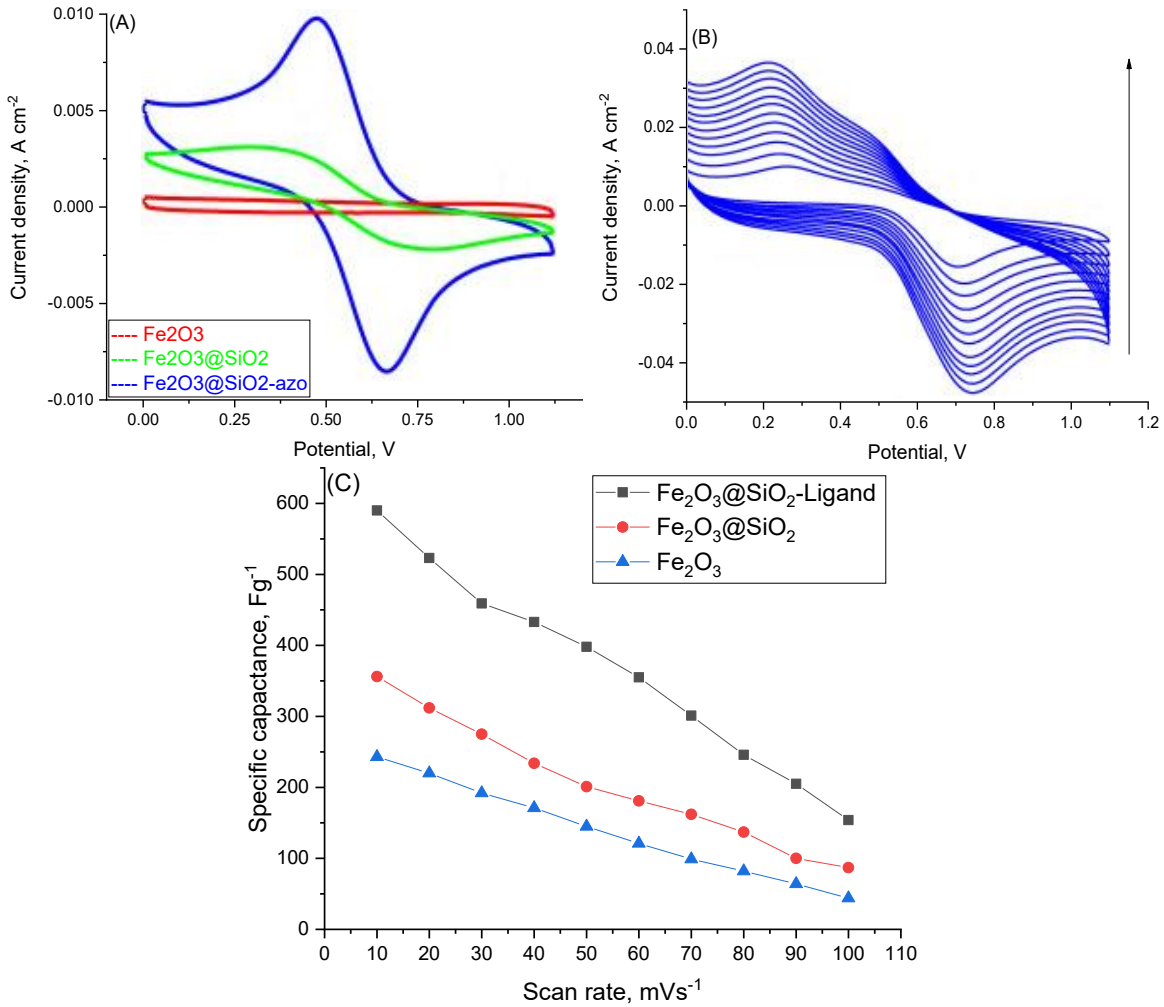

Figure 8. *CVs of (A) γ-Fe_2O_3, γ-Fe_2O_3@SiO_2 and γ-Fe_2O_3@SiO_2 azo ligand electrodes at 10 mV s^{-1}, and (B) γ-Fe_2O_3@SiO_2-azo ligand electrode at different scan rates (10-100 mV s^{-1}), (C) specific capacitance of three electrodes at different scan rates*

The GCD measurements of prepared compounds (γ-Fe_2O_3, γ-Fe_2O_3@SiO_2 and γ-Fe_2O_3@SiO_2-2-(2--benzothiazolyl azo)-4-methoxyaniline) were performed at different current densities (0-10 mA g^{-1}) in the presence of 1 M Na_2SO_4 as the electrolyte solution. The results show that discharge times are decreased with increasing current density due to increased drop voltage. At different current densities, the specific capacitance value was calculated using the following equation [35]:

$$C_{sp} = \frac{I \Delta t}{m \Delta V} \quad (2)$$

where *I* is the current density in the GCD experiment, Δt is discharge time, *m* is the mass of active material (0.5 g) and ΔV is the potential window. The specific capacitance values of prepared compounds at different current densities are summarized in Table 2.

Table 2. *Specific capacitance values obtained by GCD measurements at different current densities*

Current density, A g^{-1}	Specific capacitance, F g^{-1}	
	Electrodes	
	γ-Fe_2O_3	γ-Fe_2O_3@SiO_2-2-(2-benzothiazolyl azo)-4-methoxyaniline
1	273	580
2.5	214	513
5	167	458
10	123	399

The results show that specific capacitance is promoted by incorporating 2-(2-benzothiazolyl azo)-4-methoxyaniline with γ-Fe_2O_3@SiO_2 compared with γ-Fe_2O_3 electrode because of providing more active sites for transferring electrons inside the electrodes and many sites for storing energy. On the other hand, the results show a decrease in the specific capacitance with increasing current density because there is not enough time for ions to arrive at the surface of the electrode and work in electrochemical reactions [36-39].

The cycling stabilities of γ-Fe_2O_3@SiO_2-2-(2-benzothiazolyl azo)-4-methoxyaniline and γ-Fe_2O_3 electrodes are investigated by GCD measurements (Figure 9) at 10 A/g current density for 1000 cycles. Pure γ-Fe_2O_3 electrode shows lower stability compared with the functionalized electrode due to its destruction *via* large current, discharge and circular charge [39]. After 750 cycles at 10 A g^{-1}, the functionalized electrode exhibited higher stability compared with γ-Fe_2O_3, with 92 % of initial capacitance remaining after 1000 cycles, which indicates a good role of the azo compound in the cycle stability of the electrode.

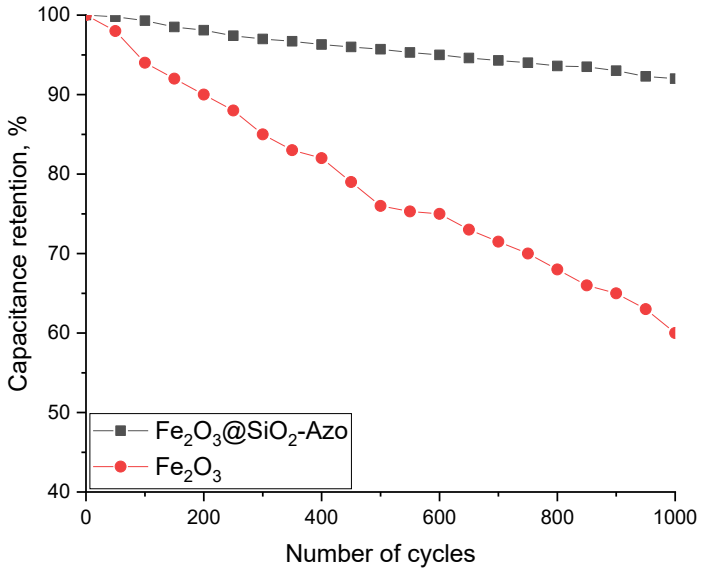

Figure 9. *Cycling stability of γ-Fe_2O_3 and γ-Fe_2O_3@SiO_2 -azo ligand electrodes*

From electrochemical measurements, our prepared hybrid nanocomposite shows a very good capability to store the charges and electric energy (580 F g^{-1}) when comparing it with other polymeric and binary oxide compounds (Table 3). It can be noted that the synthesized γ-Fe_2O_3@SiO_2-2-(2-

-benzothiazolyl azo)-4-methoxyaniline) hybrid nanocomposite has interesting electrochemical properties already reported in the literature.

***Table 3. S**pecific capacitance for some iron oxide composites (current density = 1 A g^{-1})*

Compounds	Specific capacitance, F g^{-1}	Reference
Iron oxide@SiO_2@PolyFc	675	[40]
Porous-Fe_2O_3@C nanowire	280	[41]
Iron oxide@SiO_2-bis(aminopyridine)-Cu	263	[42]
Flexible iron oxide@C/MnO_2	306	[43]
Iron oxide/reduced graphene oxide	480	[44]
γ-Fe_2O_3@SiO_2-2-(2-benzothiazolyl azo)-4-methoxyaniline	580	This study

Conclusion

Stöber method was used to prepare γ-Fe_2O_3@SiO_2 core-shell nanocomposite that was functionalized by 2-(2-benzothiazolyl azo)-4-methoxyaniline modified-MNPS, and characterized by different techniques such as XRD, XPS, TEM, FESEM-EDX-mapping, while the electrochemical performance CV, GCD and EIS. Electrochemical characterization showed good cycling stability, good rate capability and high specific capacitance of 580 F g^{-1} at 1 A g^{-1} current density. After 100 cycles, the specific capacitance of γ-Fe_2O_3@SiO_2-azo ligand electrodes is reduced to 92 % of retention capacitance. The good electrochemical performance and simple and easy fabrication of γ-Fe_2O_3@SiO_2-azo suggest that this material is a promising capacitor electrode.

***Conflicts of Interest:** The authors declare no conflict of interest.*

References

[1] A. Kathalingam, S. Ramesh, A. Sivasamy, H. Kim, H. Kim, Supercapacitor performance of MnO_2/$NiCo_2O_4$@N-MWCNT hybrid nanocomposite electrodes, *Journal of Sol-Gel Science and Technology* **91** (2019) 154-164. https://doi.org/10.1007/s10971-019-05032-0

[2] B.R. Wiston, M. Preethi, M. Ashok, Supercapacitor Performance of β-Cobalt Hydroxide Prepared via a One-Pot Hydrothermal Method, *Journal of Electronic Materials* **52** (2023) 1644-1651. https://doi.org/10.1007/s11664-022-09988-8

[3] Y. Lin, S. Zhang, L. Guan, J. Tao, Prospect of Ni-related metal oxides for high-performance supercapacitor electrodes, *Journal of Materials Science* **56** (2021) 1897-1918. https://doi.org/10.1007/s10853-020-05408-6

[4] R. Garg, A. Agarwal, M. Agarwal, Performance of Copper Sulfide Hollow Rods in a Supercapacitor Based on Flexible Substrates, *Journal of Electronic Materials* **50** (2021) 6974-6980. https://doi.org/10.1007/s11664-021-09162-6

[5] Z. H Mahmoud, R. A. AL-Bayati, A. A Khadom, Electrochemical Photocatalytic Degradation of Rhodamine B Dye by Sm^{3+} doped Titanium Dioxide (Sm-TiO_2) in Natural Sunlight Exposure, *International Journal of Electrochemical Science* **16** (2021) 211241. https://doi.org/10.20964/2021.12.43

[6] S. Singhal, A. Shukla, Improved electrochemical performance of supercapacitors by utilizing ternary Pd-AC-doped NiO nanostructure as an electrode material, *Journal of Solid State Electrochemistry* **24** (2020) 1271-1282. https://doi.org/10.1007/s10008-020-04615-0

[7] K. Dong, Z. Yang, D. Shi, M. Chen, W. Dong, Nitrogen-doped carbon boosting Fe_2O_3 anode performance for supercapacitors, *Journal of Materials Science: Materials in Electronics* **33** (2022) 13547-13557. https://doi.org/10.1007/s10854-022-08289-4

[8] C. Wu, Z. Zhang, Z. Chen, Z. Jiang, H. Li, H. Cao, Y. Liu, Y. Zhu, Z. Fung, X. Yu, Rational design of novel ultra-small amorphous Fe_2O_3 nanodots/graphene heterostructures for all-solid-

state asymmetric supercapacitors, *Nano Research* **14** (2021) 953-960. https://doi.org/10.1007/s12274-020-3131-z

[9] P. de la Presa, Y. Luengo, M. Multigner, R. Costo, M. Morales, G. Rivero, A. Hernando, Study of heating efficiency as a function of concentration, size, and applied field in γ-Fe_2O_3 nanoparticles, *Journal of Physical Chemistry C* **116** (2012) 25602-25610. https://doi.org/10.1021/jp310771p

[10] O. Lemine, K. Omri, M. Iglesias, V. Velasco, P. Crespo, P. de la Presa, L. el Mir, H. Bouzid, A. Yousif, A. Al-Hajry, γ-Fe_2O_3 by sol-gel with large Nps size for magnetic hyperthermia application, *Journal of Alloys and Compounds* **607** (2014) 125-131. https://doi.org/10.1016/j.jallcom.2014.04.002

[11] W. A. Ibrahim, Z. H. Mahmoud, Synthesis and characterization of new Fe-complex and its nanoparticle oxide using the novel photolysis method, *International Journal of Pharmaceutical and Phytopharmacological Research* **8** (2018) 57-61. https://eijppr.com/iAdYMeR

[12] N. S. Al-Obaidi, Z. H. Mahmoud, A. A. Frayyih, A.S. Ali, F. K Ali, Evaluating the electric properties of poly aniline with doping ZnO and α-Fe_2O_3 nanoparticles, *Pharmacophore* **9** (2018) 61-67. https://pharmacophorejournal.com/storage/models/article/STduXQmygcDo2fmBXOqV3fSfpGqvV6VKy883UkqgJ4CnxiEsnw4XusWVyIEw/evaluating-the-electric-properties-of-poly-aniline-with-doping-zno-and-fe2o3-nanoparticles.pdf

[13] H. Shao, Y. Zhou, J. Qi, P. Hu, J. He, Characterization of Fe_3O_4/γ-Fe_2O_3@SiO_2 Core-Shell Structure Composite Magnetic Fluid by Microemulsion Method, *Journal of Superconductivity and Novel Magnetism* **32** (2019) 247-252. https://doi.org/10.1007/s10948-018-4910-6

[14] H. Zhang, Y. Ye, Z. Li, Y. Chen, P. Deng, Y. Li, Synthesis of Fe_2O_3-$Ni(OH)_2$/graphene nanocomposite by one-step hydrothermal method for high-performance supercapacitor, *Journal of Materials Science* **51** (2016) 2877-2885. https://doi.org/10.1007/s10853-015-9596-6

[15] W. Gao, Y. Li, J. Zhao, Z. Zhang, W. Tang, J. Wang, Z. Wu, Z. Li, Design and Preparation of Graphene/Fe_2O_3 Nanocomposite as Negative Material for Supercapacitor, *Chemical Research in Chinese Universities* **38** (2022) 1097-1110. https://doi.org/10.1007/s40242-022-1442-1

[16] Z. H. Mahmoud, M. S. Falih, O. E. Khalaf, M. A. Farhan, F. K. Ali, Photosynthesis of AgBr Doping TiO_2 Nanoparticles and degradation of reactive red 120 dye, *Journal of Advanced Pharmacy Education & Research* **8(4)** (2018) 51-55. https://japer.in/article/photosynthesis-of-agbr-doping-tio2-nanoparticles-and-degradation-of-reactive-red-120-dye

[17] M. A. Farhan, Z. H. Mahmoud, M. S. Falih, Synthesis and characterization of TiO_2/Au nanocomposite using UV-Irradiation method and its photocatalytic activity to degradation of methylene blue, *Asian Journal of Chemistry* **30(5)** (2018) 1142-1146. https://doi.org/10.14233/ajchem.2018.21256

[18] Z. H. Mahmoud, R. A. AL-Bayati, A. A Khadom, The efficacy of samarium loaded titanium dioxide (Sm:TiO_2) for enhanced photocatalytic removal of rhodamine B dye in natural sunlight exposure, *Journal of Molecular Structure* **1253** (2022) 132267. https://doi.org/10.1016/j.molstruc.2021.132267

[19] R. Eisavi, K. Naseri, Preparation, characterization and application of $MgFe_2O_4$/Cu nanocomposite as a new magnetic catalyst for one-pot regioselective synthesis of β-thiol-1,4-disubstituted-1,2,3-triazoles, *RSC Advances* **11(22)** (2021) 13061-13076. https://doi.org/10.1039/D1RA01588E

[20] M. Mahmoudzadeh, E. Mehdipour, R. Eisavi, $MgFe_2O_4$@SiO_2-$PrNH_2$/Pd/bimenthonoxime core-shell magnetic nanoparticles as a recyclable green catalyst for heterogeneous Suzuki cross-coupling in aqueous ethanol, *Journal of Coordination Chemistry* **72(5-7)** (2019) 841-859. https://doi.org/10.1080/00958972.2019.1590562

[21] M. Ibrahim, H.N. Abdelhamid, A.M. Abuelftooh, S.G. Mohamed, Z. Wen, X. Sun, Covalent organic frameworks (COFs)-derived nitrogen-doped carbon/reduced graphene oxide nanocomposite as electrodes materials for supercapacitors, *Journal of Energy Storage* **55** (2022) 105375. https://doi.org/10.1016/j.est.2022.105375

[22] A. A. Qaiser, M. M. Hyland, D. A. Patterson, Surface and charge transport characterization of polyaniline−cellulose acetate composite membranes, *The Journal of Physical Chemistry B* **115(7)** (2011) 1652-1661. https://doi.org/10.1021/jp109455m

[23] M. Ibrahim, M. G. Fayed, S. G. Mohamed, Z. Wen, X. Sun, H.N. Abdelhamid, High-Performance Lithium-Ion Battery and Supercapacitors Using Covalent Organic Frameworks (COFs)/Graphitic Carbon Nitride (g-C_3N_4)-Derived Hierarchical N-Doped Carbon, *ACS Applied Energy Materials* **5(10)** (2022) 12828-12836. https://doi.org/10.1021/acsaem.2c02415

[24] B.-X. Zou, Y. Liang, X.-X. Liu, D. Diamond, K.-T. Lau, Electrodeposition and pseudocapacitive properties of tungsten oxide/polyaniline composite, *Journal of Power Sources* **196(10)** (2011) 4842-4848. https://doi.org/10.1016/j.jpowsour.2011.01.073

[25] F. Davar, M. Salavati-Niasari, Z. Fereshteh, Synthesis and characterization of SnO_2 nanoparticles by thermal decomposition of new inorganic precursor, *Journal of Alloys and Compounds* **496(1-2)** (2010) 638-643. https://doi.org/10.1016/j.jallcom.2010.02.152

[26] S. Yao, S. Xue, S. Peng, M. Jing, X. Qian, X. Shen, T. Li, Y. Wang, Synthesis of graphitic carbon nitride at different thermal-pyrolysis temperature of urea and its application in lithium-sulfur batteries, *Journal of Materials Science: Materials in Electronics* **29** (2018) 17921-17930. https://doi.org/10.1007/s10854-018-9906-2

[27] Y. A. Kumar, B. A. Al-Asbahi, M. R. Pallavolu, S. S. Rao, R. R. Nallapureddy, S. Ramakrishna, Multiple structural defects in poor crystalline nickel-doped tungsten disulfide nanorods remarkably enhance supercapacitive performance, *International Journal of Energy Research* **46(10)** (2022) 14227-14239. https://doi.org/10.1002/er.8137

[28] Y. A. Kumar, H. T. Das, P. R. Guddeti, R. R. Nallapureddy, M. R. Pallavolu, S. Alzahmi, I. M. Obaidat, Self-Supported Co_3O_4@Mo-Co_3O_4 Needle-like Nanosheet Heterostructured Architectures of Battery-Type Electrodes for High-Performance Asymmetric Supercapacitors, *Nanomaterials* **12(14)** (2022) 2330. https://doi.org/10.3390/nano12142330

[29] Y. A. Kumar, K. D. Kumar, H.-J. Kim, Reagents assisted $ZnCo_2O_4$ nanomaterial for supercapacitor application, *Electrochimica Acta*, **330** (2020) 135261. https://doi.org/10.1016/j.electacta.2019.135261

[30] Y. A. Kumar, S. Sambasivam, S. A. Hira, K. Zeb, W. Uddin, T. N. V. Krishna, K. D. Kumar, I. M. Obaidat, H.-J. Kim, Boosting the energy density of highly efficient flexible hybrid supercarpacitors via selective integration of hierarchical nanostructured energy materials, *Electrochimica Acta* **364** (2020) 137318. https://doi.org/10.1016/j.electacta.2020.137318

[31] Z. H Mahmoud, R. A. AL-Bayati, A. A Khadom, Synthesis and supercapacitor performance of polyaniline-titanium dioxide-samarium oxide (PANI/TiO_2-Sm_2O_3) nanocomposite, *Chemical Papers* **76** (2022) 1401-1412. https://doi.org/10.1007/s11696-021-01948-6

[32] T. T. Anh, V. M. Thuan, D. H. Thang, B. T. Hang, Effect of Fe_2O_3 and Binder on the Electrochemical Properties of Fe_2O_3/AB (Acetylene Black) Composite Electrodes, *Journal of Electronic Materials*, **46** (2017) 3458-3462. https://doi.org/10.1007/s11664-016-5221-y

[33] S. S. Patil, K. V. Harpale, S. P. Koiry, K. R. Patil, D. K. Aswal, M. A. More, Multifunctional polyaniline-tin oxide (PANI-SnO_2) nanocomposite: Synthesis, electrochemical, and field emission investigations, *Journal of Applied Polymer Science* **132(5)** (2015) 41401. https://doi.org/10.1002/app.41401

[34] F. Xie, M. Zhou, G. Wang, Q. Wang, M. Yan, H. Bi, Morphology dependent electrochemical performance of nitrogendoped carbon dots@polyaniline hybrids for supercapacitors,

International Journal of Hydrogen Energy **43(13)** (2019) 7529-7540. https://doi.org/10.1002/er.4678

[35] L. Yu, G. Z. Chen, Supercapatteries as high-performance electrochemical energy storage devices, *Electrochemical Energy Reviews* **3** (2020) 271-285. https://doi.org/10.1007/s41918-020-00063-6

[36] J. Ben, Z. Song, X. Liu, W. Lu, X. Li, Fabrication and Electrochemical Performance of PVA/CNT/PANI flexible films as electrodes for supercapacitors, *Nanoscale Research Letters* **15** (2020) 151. https://doi.org/10.1186/s11671-020-03379-w

[37] L. Zhang, H. Xia, S. Liu, Y. Zhou, Y. Zhao, W. Xie, Nickel-cobalt hydroxides with tunable thin-layer nanosheets for high-performance supercapacitor electrode, *Nanoscale Research Letters* **16** (2021) 83. https://doi.org/10.1186/s11671-021-03543-w

[38] R. Eisavi, F. Ahmadi, Fe_3O_4@SiO_2-PMA-Cu magnetic nanoparticles as a novel catalyst for green synthesis of β-thiol-1,4-disubstituted-1,2,3-triazoles, *Scientific Reports* **12** (2022) 11939. https://doi.org/10.1038/s41598-022-15980-3

[39] J. Wan, A. Pang, D. He, A high-performance supercapacitor electrode based on three-dimensional poly-rowed copper hydroxide nanorods on copper foam, *Journal of Materials Science: Materials in Electronics* **29** (2018) 2660-2667. https://doi.org/10.1007/s10854-017-8192-8

[40] E. Payami, M. A. Keynezhad, K. D. Safa, R. Teimuri-Mofrad, Development of high-performance supercapacitor based on Fe_3O_4@SiO_2@PolyFc nanoparticles via surface-initiated radical polymerization, *Electrochimica Acta* **439** (2023) 141663. https://doi.org/10.1016/j.electacta.2022.141663

[41] Y. Dong, L. Xing, K. Chen, K. Wu, Porous Fe_2O_3@C nanowire arrays as flexible supercapacitors electrode materials with excellent electrochemical performances, *Nanomaterials* **8(7)** (2018) 487. https://doi.org/10.3390/nano8070487

[42] M. A. Mustafa, Q. A. Qasim, A. B. Mahdi, S. E. Izzat, Y. S. Alnassar, E. S. Abood, Z. J. alhakim, Z. H. Mahmoud, A. M. Rheima, H. N. K. Al-Salman, Supercapacitor performance of Fe_3O_4 and Fe_3O_4@ SiO_2-bis (aminopyridine)-Cu hybrid nanocomposite, *International Journal of Electrochemical Science* **17** (2022) 221057. http://doi.org/10.20964/2022.10.49

[43] N. Iqbal, X. Wang, A. A. Babar, Flexible Fe_3O_4@Carbon Nanofibers Hierarchically Assembled with MnO_2 Particles for High-Performance Supercapacitor Electrodes, *Scientific Reports* **7** (2017) 15153. https://doi.org/10.1038/s41598-017-15535-x

[44] W. Shi, J. Zhu, D. H. Sim, Y. Y. Tay, Z. Lu, X. Zhang, Y. Sharma, M. Srinivasan, H. Zhang, H. H. Hng, Q. Yan, Achieving high specific charge capacitances in Fe_3O_4/reduced graphene oxide nanocomposites, *Journal of Materials Chemistry* **21** (2011) 3422-3427. https://doi.org/10.1039/c0jm03175e